



## Ankaramite from Tenerife: a novel geothermobarometric approach to gain insights into the depth of a magma plumbing system

Lorenzo Barni<sup>1</sup>, Simone Tommasini<sup>1,2</sup>, Marta Morana<sup>1</sup>, Riccardo Avanzinelli<sup>1</sup>, Tiziano Catelani<sup>3</sup>, and Luca Bindi<sup>1,2</sup>

<sup>1</sup>Department of Earth Sciences, Università degli Studi di Firenze, Via G. La Pira 4, 50121 Firenze, Italy

<sup>2</sup>C.N.R. – Istituto di Geoscienze e Georisorse, Università degli Studi di Firenze,  
Via G. La Pira 4, 50121 Firenze, Italy

<sup>3</sup>MEMA – Centro di Servizi di Microscopia Elettronica e Microanalisi, Università degli Studi di Firenze,  
Via G. Capponi 3/r, 50121 Firenze, Italy

**Correspondence:** Luca Bindi (luca.bindi@unifi.it)

Received: 16 January 2025 – Revised: 1 August 2025 – Accepted: 16 August 2025 – Published: 17 October 2025

**Abstract.** This study investigates the magma plumbing system of the Miocene volcano shield stage of Tenerife (Canary Islands) through a geothermobarometric analysis of clinopyroxenes in ankaramite dykes and lavas from the Teno and Roque del Conde massifs. Ankaramites, characterized by a high phenocryst content of olivine and clinopyroxene, provide valuable insights into magma storage and transport processes. Two different methods have been applied to estimate the pressure and temperature of crystallization of clinopyroxenes: (i) a novel machine learning geothermobarometer and (ii) a geobarometer that uses their structural parameters ( $V_{\text{cell}}$  and  $V_{\text{M1}}$  polyhedron). The results yielded a pressure distribution between 0 and 8 kbar with a difference between clinopyroxene cores and rims, reflecting a multi-level plumbing system with evidence for the progressive ascent and crystallization of magmas. Further considerations of aluminium incorporation into the tetrahedral site and zonation patterns of clinopyroxene cores revealed three groups with distinct  $P$ – $T$  paths, which are *Low-T*, *High-T*, and *Low-P* clinopyroxenes. *Low-T* clinopyroxenes are the largest ones (up to few centimetres in size) and exhibit resorbed and patchy zonation. This group represents a relatively cold crystal mush formed from a more hydrated magma, accumulated during a long residence time in disequilibrium conditions, as testified by crystal habits. *High-T* clinopyroxenes show normal zonation pattern and consist of small crystals (1–2 mm in size) directly crystallized from a less hydrated carrier magma during its ascent from depth (> 20 km b.s.l.). This magma, which tore away part of the crystal mush bodies, acted as the transport agent of these two suites of crystals up to the shallower crustal reservoirs (0–7 km). At these depths, clinopyroxene cores of the *Low-P* group crystallized in the same  $P$ – $T$  conditions as those of the rim domain, in a chemical disequilibrium regime, proved by resorbed and patchy textures. In this scenario, ankaramites witness the occurrence of a heterogeneous cargo of clinopyroxenes that formed at different depths in the plumbing system of the Teno and Roque del Conde massifs during the volcano shield stage. The results of our research extend previous geothermobarometric studies and refine the understanding of the ankaramite plumbing system of Tenerife. Our data are consistent with the plumbing systems of other shield volcanoes of the Canary Islands and Hawaii and boost the application of machine learning approaches in revealing the anatomy of volcano plumbing systems.

## 1 Introduction

Studying the Earth's interior is paramount to understanding the dynamic processes that shaped the geological evolution of our planet. Volcanic eruptions provide critical windows into these hidden domains, as the crystal cargos of ascending magmas preserve physical and chemical fingerprints of their formation environments. Volcanic rocks act as natural probes, containing mineral assemblages, melt inclusions, and textural features that record the pressure–temperature–composition ( $P$ – $T$ – $X$ ) conditions of magma storage and transport (e.g. Ubide et al., 2021).

Geothermobarometry represents an essential technique for decoding these magmatic archives and reconstructing the thermal conditions and anatomy of volcanic plumbing systems (e.g. Putirka, 2008). This approach has revolutionized our understanding of magma dynamics beneath ocean island volcanoes, where complex plumbing systems often involve multi-level storage regions and mixing processes (e.g. Cashman et al., 2017). In this work, we explore the challenges and insights offered by geothermobarometry in the context of a very peculiar kind of volcanic rock: ankaramite. Ankaramite is a field name nomenclature (Lacroix, 1916) that refers to an effusive mafic rock (basanite, picrobasalt, alkali basalt) with a phenocryst content (olivine and clinopyroxene) greater than 30%–40%, in some cases reaching 50%–60%. Ankaramites typically occur in two geodynamic settings, volcanic arcs and oceanic intraplate volcanoes, although minor occurrences in mid-ocean ridge settings have also been reported (e.g. Schmidt et al., 2004). Most studies have been focused on ankaramites outcropping at Maui in the Hawaiian Islands (Chatterjee et al., 2005; Hammer et al., 2016) and the Canary Islands hotspot (Klügel et al., 2005; Galipp et al., 2006; Longpré et al., 2008, 2009). The aims of this study are to shed light on the ankaramite plumbing system of the Teno and Roque del Conde massifs on Tenerife (Canary Islands) and to compare the results obtained with two independent geothermobarometers based upon clinopyroxene crystal structure (Nimis and Ulmer, 1998) and clinopyroxene-only machine learning techniques (Chicchi et al., 2023) with previous estimates (Longpré et al., 2008).

### 1.1 Geological background

The Canary archipelago is made up by seven NE–SW-trending islands located on the Atlantic oceanic crust of Jurassic age (Müller et al., 1997) at some 300 km off the coast of Morocco (Fig. 1). The age of the Islands (McDougall and Schmincke, 1976; Ancochea et al., 1990; Guillou et al., 1996, 2004) is progressively younger going from the NE (~22 Ma at Fuerteventura, Lanzarote) to the SW end of the archipelago (~2 Ma at El Hierro, La Palma). Tenerife is the largest of the Canary Islands and has a complex volcanological history. The subaerial volcanic activity



**Figure 1.** Sketch map of Tenerife, Canary Islands (from Google Maps). The colours on the map highlight the main outcrop areas of the Miocene shield volcano: Teno (red), Roque del Conde (yellow), and Anaga (green). Yellow stars indicate the two sampling localities. The inset illustrates the position of the Canary Islands off the coast of southern Morocco.

started at ~12 Ma as a volcano shield stage (Fig. 1). Fúster et al. (1968), Ancochea et al. (1990), and Thirlwall et al. (2000) suggested that the shield stage was formed by three separated basaltic shield complexes, namely, Teno, Roque del Conde, and Anaga. However, recent studies have supported a scenario with a unique central shield volcano now outcropping at the corners of the island (Ablay and Kearey, 2000; Araña et al., 2000; Guillou et al., 2004; Sainz-Maza Aparicio et al., 2019). The stratigraphic sequence of this shield volcano is part of the Old Basaltic Series (OBS; Fúster et al., 1968; Ancochea et al., 1990) and defines the oldest exposed rocks at Tenerife (Fig. 1). Some key features of Roque del Conde, Anaga, and Teno are listed below, with emphasis on the Teno massif because most of the samples used in this work come from this part of the island.

Roque del Conde represents the central part of the shield volcano, and its formation ranges from 11.9 to 8.9 Ma (Thirlwall et al., 2000; Guillou et al., 2004). The products of the OBS recognized in the Roque del Conde sequence include picrobasalt, basalt, basanite, hawaiite, mugearite, and benmoreite (Thirlwall et al., 2000). The Anaga massif is mainly composed of a complex sequence of alkaline basaltic lava flows, with abundant volcanoclastic layers, intruded by subvolcanic bodies of basalts, trachybasalts, trachytes, and phonolites (Ancochea et al., 1990). The stratigraphic series has a total thickness of about 1000 m and formed at 8.4–3.9 Ma (Thirlwall et al., 2000). The Teno massif contributed to the building of the island during the Miocene (6.4–5.1 Ma; Thirlwall et al., 2000). The stratigraphic sequence starts with a series of basaltic lavas and dykes (Masca Formation; Ancochea et al., 1990). The first collapse event (Masca Uncon-

formity) is recognizable at the top of the sequence, and it is followed by the filling of the collapse scar with the Carrizales Formation. This kind of eruption cycle, comprising a first episode of volcanic activity and a subsequent collapse of the edifice, is typical of this volcano. On top of the Carrizales Formation there is another collapse event (Carrizales Unconformity; Walter and Schmincke, 2002), which was in turn followed by a subsequent episode of volcanic activity (El Palmar–Los Gigantes; Guillou et al., 2004). Previous studies at Tenerife found ankaramitic lavas in the Teno shield volcano stratigraphic sequences and correlated their occurrence to the flank collapses (Longpré et al., 2009). This process can overcome the problem of erupting high-density magma such as ankaramite (ca.  $3 \text{ t m}^{-3}$ ; Longpré et al., 2009) because the fast lithostatic decompression of the system coupled with the rapid exsolution of volatiles during flank collapse is liable to triggering the eruption of dense magma with a large (30 vol %–40 vol %) phenocryst content (Longpré et al., 2009).

## 2 Samples and analytical methods

The studied ankaramites are massive lavas and dykes collected from two distinct outcrops in two parts of the island: five samples near Masca (Ank-1, Ank-2, Ank-3, Ank-4, Ank-5), belonging to the Teno massif (Figs. 1, 2), and one sample (Ank-7) from Roque del Conde, near Granadilla (see Table S1 in the Supplement for coordinates and outcropping characteristics of the samples). All the rocks have porphyritic texture with large clinopyroxene and olivine phenocrysts (up to 1–3 cm in length) embedded in a microcrystalline groundmass (Fig. 2). The textural characteristics of the crystals were initially studied using a ZEISS EVO MA15 scanning electron microscope (SEM) on polished mounts (Fig. S1 in the Supplement). Two to three fragments of clinopyroxene crystals from each rock sample were then selected for the single-crystal X-ray diffraction experiments, mainly on the basis of the absence of twinning. A total of 14 fragments (ranging from 20 to 100  $\mu\text{m}$  in size) from cores and rims of clinopyroxenes were extracted using a needle and mounted on a support with glue. Single-crystal X-ray diffraction data were collected on a Bruker-D8 Venture diffractometer equipped with a Photon III detector and using Mo- $K\alpha$  radiation. The chemical formulae of the refined clinopyroxenes were calculated according to the procedure proposed by Dal Negro et al. (1982), and the results of the structure refinements are given in Tables S2 and S3. The refinement of the site scattering at the structural sites allowed us to obtain reliable chemical partitioning into the T, M1, and M2 sites, leading to a correct distribution of  $\text{Fe}^{2+}$  and  $\text{Mg}^{2+}$  between the M1 and M2 polyhedra (Dal Negro et al., 1982). Quantitative chemical compositions were then determined using a JEOL-JXA 8230 electron microprobe on the same polished mounts (Fig. S1). Measuring conditions were set up at 15 kV with a

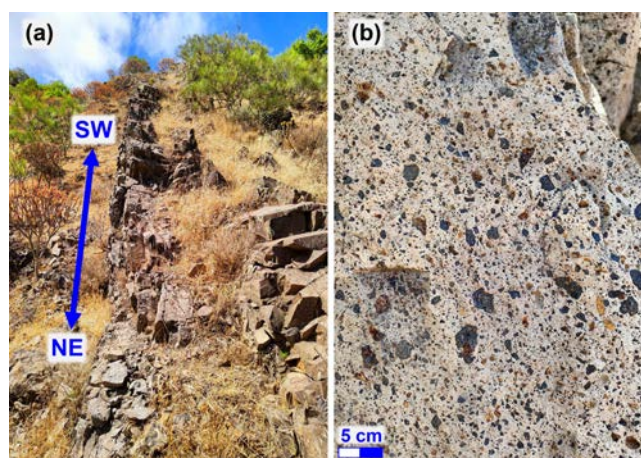


**Figure 2.** Ankaramites from the Teno massif. (a) Outcrop of a SW–NE-trending ankaramitic dyke  $\sim 1.5$  m wide; (b) macroscopic photo of a massive lava flow with huge ( $> 1$  cm) phenocrysts of clinopyroxene and olivine.

beam current of 20 nA for silicates (olivine, clinopyroxene, and feldspar). The beam diameter was adjusted at 3  $\mu\text{m}$  for clinopyroxene and olivine and 5  $\mu\text{m}$  for feldspar. Clinopyroxene formulae and components (Table S4) were calculated on the basis of 4 cations, and  $\text{Fe}^{2+}/\text{Fe}^{3+}$  was adjusted to maintain charge balance (Chicchi et al., 2023, for details).

### 2.1 Geothermobarometry

A quantitative assessment of intensive variables of clinopyroxene crystallization was performed using two different geothermobarometers. The first one, GAIA (Chicchi et al., 2023), is based upon machine learning techniques which are gaining widespread relevance and are expected to yield a significant methodological shift in Earth sciences applications (e.g. Petrelli, 2023). GAIA is a novel feedforward neural network trained with a database of  $\sim 5600$  experimental petrology clinopyroxene analyses from the Library of Experimental Phase Relations (Hirschmann et al., 2008) complemented by more recent compilations and filtered according to several parameters to check for analyses' quality (see Chicchi et al., 2023, for details). The  $P$  and  $T$  errors of this method are  $\pm 1$  kbar and  $\pm 30$   $^{\circ}\text{C}$  (1 SEE, standard error estimate), respectively. The second method is a geobarometer based on the crystal chemistry and structure of clinopyroxenes (Nimis and Ulmer, 1998) and requires the knowledge of the temperature to yield valuable pressure estimates. In this study we adopted the temperature obtained with the GAIA geothermobarometer. The pressure for each crystal was calculated following the procedure outlined by Nimis and Ulmer (1998) calibrated for the MA compositional range (mildly alkaline series from alkali basalt to trachyandesite, including mildly alkaline and transitional melts of the shoshonitic series) with an error of  $\pm 2$  kbar (1 SD). Overall, 222 clinopyroxene anal-

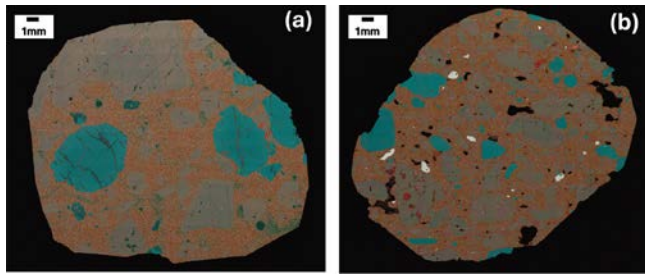


**Figure 3.** X-ray compositional maps (cameo: Ca, red; Mg, light blue; Al, orange) highlighting the two different textures representative of the entire suite of the studied samples. Olivine and clinopyroxene crystals are light blue and light brown, respectively. (a) Large and few clinopyroxene and olivine crystals (Ank-1), as opposed to (b) small and abundant clinopyroxene and olivine crystals (Ank-7) in a microcrystalline groundmass.

yses were selected as input for the GAIA geothermobarometer (Table S4), whereas 14 structure refinements were used to calculate the crystallization pressure with the Nimis and Ulmer (1998) geobarometer (Table S5).

### 3 Results

#### 3.1 Rock texture and crystal chemistry

Ankaramite samples exhibit well-defined phenocrysts of olivine and clinopyroxene dispersed in a microcrystalline groundmass mainly composed of plagioclase + clinopyroxene + Fe–Ti oxides (Fig. 3). Plagioclase has a labradoritic–bytownitic composition (Table S6). Samples have two different textures based upon the size and abundance of phenocrysts: (i) a rather small quantity of large (> 1 cm) olivine and clinopyroxene phenocrysts (e.g. Ank-1, Fig. 3a) and (ii) more abundant but small (< 1 cm) olivine and clinopyroxene phenocrysts (e.g. Ank-7, Fig. 3b). Teno massif samples exhibit both textures (Fig. S1), whereas the single sample from Roque del Conde displays only the second type.

##### 3.1.1 Olivine

Olivine is euhedral in all the samples (ranging from about 250  $\mu\text{m}$  to 1 cm in size) and has a homogeneous composition with a thin (a few micrometres) Fe-rich outer rim (Figs. 4, 5a, Table S7). Forsterite content varies from Fo<sub>70</sub> to Fo<sub>85</sub> mol %, with the largest frequency representing core analyses (Fo<sub>83</sub>–Fo<sub>84</sub> mol %, Fig. 5a). The rims (Fo<sub>64</sub>–75 mol %, Fig. 5a), due to their micrometric thickness, only represent a tiny part of the crystal (< 1 %; Fig. 4). Forsterite content is inversely correlated to the atoms of Ca per formula unit (a.p.f.u.) (Fig. 5b), increasing towards the rims and suggesting a qualitative shallower depth of crystallization than the cores (Brey and Kohler, 1990). No significant differences were observed between the samples of the Teno and Roque del Conde massifs.

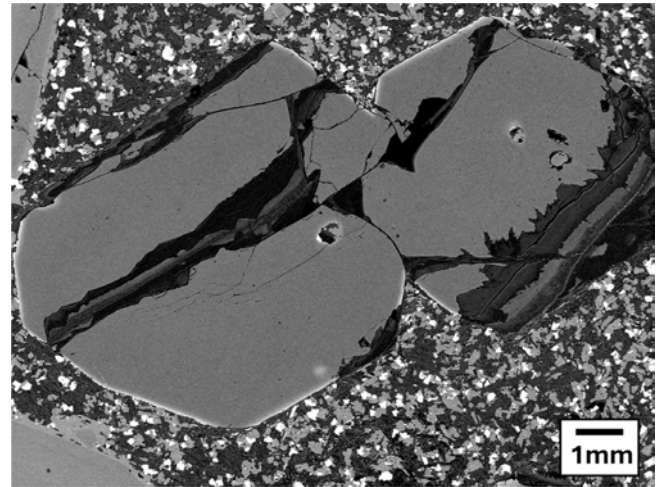


**Figure 4.** Backscattered electron image of two olivine crystals characterized by a homogeneous Fo-rich (ca. Fo<sub>80</sub> mol %) composition with a thin Fo<sub>70</sub> mol % rim. These crystals also contain iddingsite veins.

Furthermore, a few crystals also have some minor iddingsite veins (Fig. 4) caused by hydrothermal alteration (Delvigne et al., 1979).

#### 3.2 Clinopyroxene and geothermobarometry

Clinopyroxene is the most abundant phase in all the samples. Crystals reach centimetric dimensions (1–2 cm), have euhedral habit, and are diopsidic in composition (Fig. S2, Table S4). SEM analyses reveal three types of clinopyroxene phenocrysts (Fig. 6): (a) normal zoned crystals, (b) crystals with partially resorbed cores, and (c) crystals with oscillatory zoning. Normal zoned clinopyroxenes are millimetric in size and are marked by a clear, sharp boundary between core and rim, with rims enriched in Fe, Ti, and Al (Fig. 6a). Resorbed (Fig. 6b) and oscillatory zoned (Fig. 6c) crystals are the largest ones (> 1 cm), with the former having marked cores with patchy structures. The site populations and the structural details of the 14 crystal fragments (both cores and rims) are reported in Tables S2 and S3. The unit-cell volume ( $V_{\text{cell}}$ ) and the volume of the M1 polyhedron ( $V_{\text{M1}}$ ) are strongly dependent on the crystallization pressure of clinopyroxene (Nimis, 1995; Nimis and Ulmer 1998). From a qualitative point of view, the  $V_{\text{M1}}$  and  $V_{\text{cell}}$  values of the analysed clinopyroxenes ( $438.68 < V_{\text{cell}} < 441.17 \text{ \AA}^3$ ,  $11.65 < V_{\text{M1}} < 11.80 \text{ \AA}^3$ ; Table S2) indicate no difference between the Teno massif and Roque del Conde. Applying volume correction for compressibility and thermal expansivity (Nimis and Ulmer, 1998), the results yield a crystallization depth < 5 kbar (Table S3). Furthermore, the slight but significant difference between the structural parameters of clinopyroxene cores and rims suggests that rims crystallized at shallower depths than cores. The  $P$ – $T$  results of

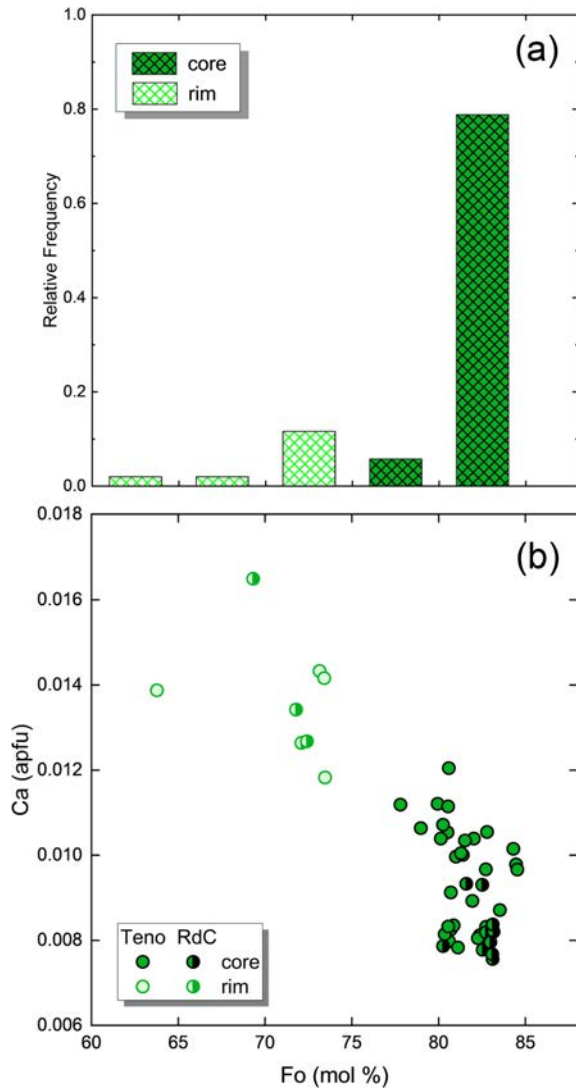


**Figure 5.** (a) Histogram of olivine core and rim composition frequency in terms of Fo mol %. (b) Fo mol % vs. Ca (a.p.f.u.) of the analysed olivines highlighting the increase in Ca towards the rim. The restricted Ca content of Roque del Conde cores with respect to Teno cores could be due to sampling bias (1 sample vs. 5 samples, Table S7).

the GAIA geothermobarometer (Table S4) are reported in Fig. 7 along with those from the Nimis and Ulmer (1998) geobarometer. Clinopyroxene cores indicate a higher pressure of crystallization than clinopyroxene rims at both the Teno and the Roque del Conde massifs. This is clearly observed in the histogram on the left-hand side of Fig. 7, representing the pressure distribution frequency obtained with the GAIA geothermobarometer – clinopyroxene rims mainly crystallized at depths between 0 and 2 kbar with a major peak at 0.5 kbar – whereas clinopyroxene cores yield a continuous crystallization between 1 and 4.5 kbar with only a few cores formed at greater depths (up to 8 kbar). The results of

these two methods are consistent with each other (blue and red symbols, Fig. 7), although  $P$  estimates based upon structural data have been performed on fewer analyses than the GAIA geothermobarometer (14 vs. 222 data points) and have a greater uncertainty ( $\pm 2$  kbar, 1 SD, Nimis and Ulmer, 1998, vs.  $\pm 1$  kbar, 1 SEE, Chicchi et al., 2023). Temperature estimates (GAIA only) yield a range from 1030 to 1190 °C, and, interestingly, a significant proportion of high- $P$  clinopyroxene cores have crystallization temperatures equal to or less than those of clinopyroxene rims (Fig. 7).

## 4 Discussion

The geothermobarometric results obtained in this study allow us to get insight into the anatomy of the plumbing system of ankaramite magmas at Tenerife during the volcano shield stage and to make a comparison with previous petrological studies (e.g. Neumann et al., 1999; Thirlwall et al., 2000; Longpré et al., 2008, 2009; Horn et al., 2022), geophysical surveys (Piña-Varas et al., 2018; Ablay and Kearey, 2000; Araña et al., 2000), and studies about the volcano shield stage on other islands of the Canary Islands (Klügel et al., 2005; Galipp et al., 2006; Weis et al., 2015; Geiger et al., 2025; Prieto-Torrell et al., 2025) and Hawaii (Hammer et al., 2016).

### 4.1 Geothermobarometry

When considered together,  $P$  and  $T$  estimates can be used to discriminate specific groups of clinopyroxene cores and rims (Fig. 8).  $P$ – $T$  estimates on clinopyroxene rims are clustered into a well-defined  $P$ – $T$  domain (0–2 kbar, 1060–1160 °C; Fig. 8). On the contrary, clinopyroxene core estimates show large  $P$ – $T$  variations, allowing us to recognize three different  $P$ – $T$  groups, which are outlined as different symbols in Fig. 8 and then maintained in the following diagrams.

- *Low- $T$* : this group comprises clinopyroxene cores that define a  $P$ – $T$  trend at relatively low temperature of crystallization, progressively increasing with pressure from ca. 1040 °C at 1.5 kbar to ca. 1110 °C at 6 kbar. Within this group, the clinopyroxene cores of Roque del Conde are confined to the low- $T$  and low- $P$  end of the trend (Fig. 8), whilst those from Teno cover the whole trend. This difference might be related to the fact that the only sample analysed of Roque del Conde is from a shallow magmatic reservoir, whilst the five samples of Teno originate from multi-level reservoirs encountered during magma ascent.
- *High- $T$* : this group is defined by clinopyroxene cores of both the Teno and the Roque del Conde massifs forming a trend at relatively constant  $T$  (ca. 1170 °C) and  $P$  decreasing from ca. 8 to 1 kbar.
- *Low  $P$* : this is a cluster of clinopyroxene cores, from both the Teno and the Roque del Conde massifs, which

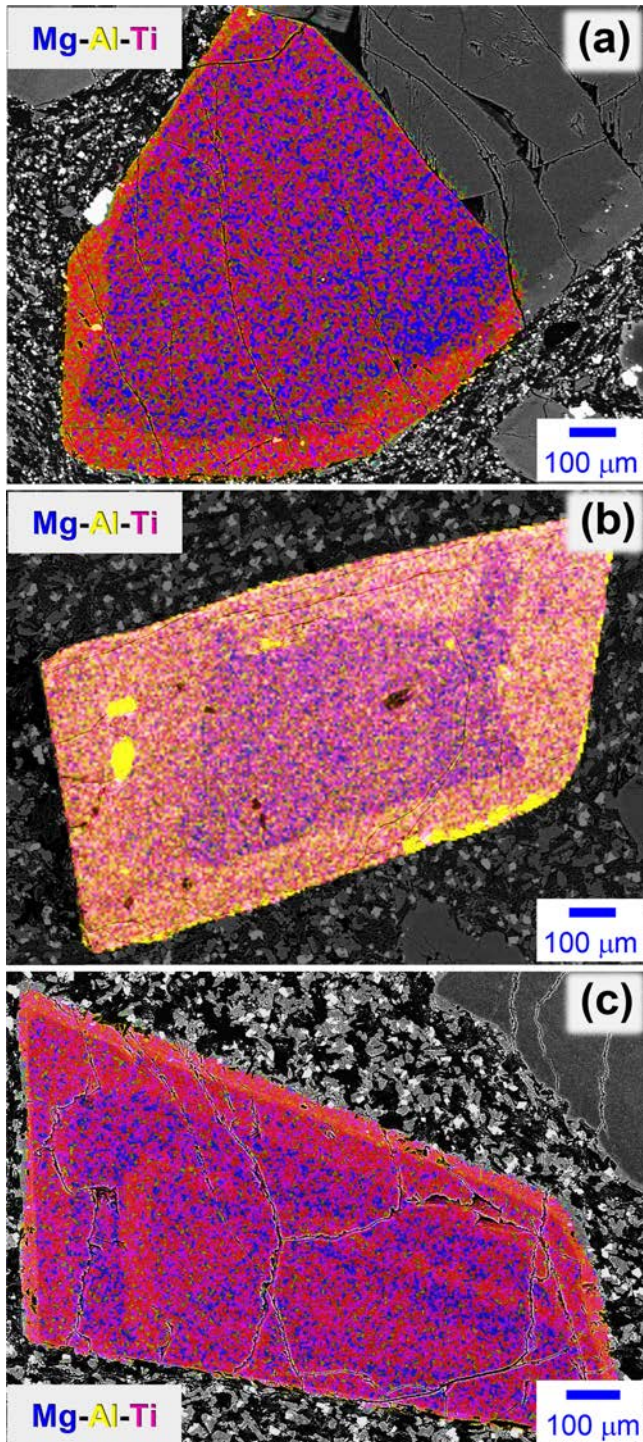


**Figure 6.** X-ray compositional maps (cameo) illustrating the three types of clinopyroxenes occurring in the studied samples: (a) normal zoned, (b) patchy-resorbed, and (c) oscillatory zoned. Normal zoned and patchy-resorbed crystals have rims with higher Al, Ti, and Fe (not shown) and lower Mg contents than cores. Oscillatory zoned crystals have multiple growth zones with alternating increases in Al, Ti, and Fe (not shown) and decreases in Mg.

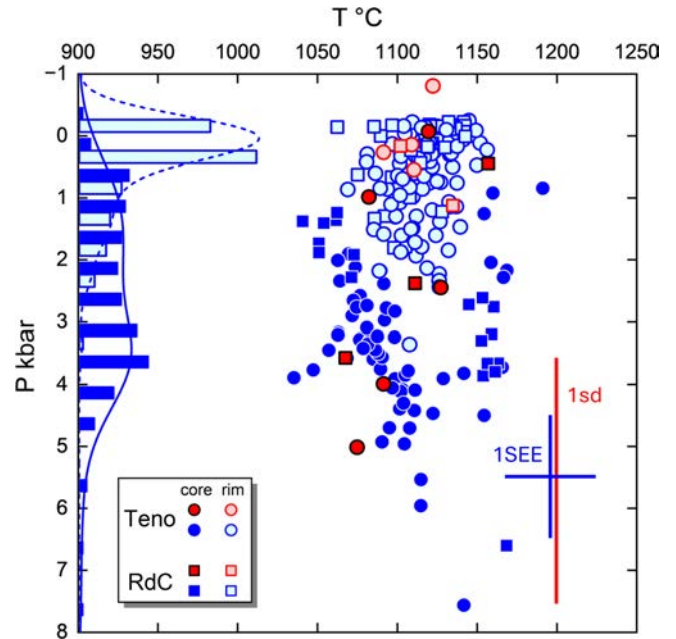


**Figure 7.**  $P$ – $T$  diagram reporting the results obtained using GAIA (blue symbols) and the Nimis and Ulmer (1998) geobarometer (red symbols). Dark- and light-coloured symbols and bars refer to the core and rim, respectively, whereas circles and squares represent Teno and Roque del Conde clinopyroxenes, respectively. The histogram of the pressure distribution frequency is reported on the left-hand side. The blue and red error bars are 1 kbar and 30 °C (1 SEE, GAIA) and 2 kbar (1 SD; Nimis and Ulmer, 1998), respectively.

crystallized under the same  $P$ – $T$  conditions as those of clinopyroxene rims (ca. 1100 °C <  $T$  < 1140 °C,  $P$  < 2 kbar; Fig. 8).

These  $P$ – $T$  groups in the clinopyroxene cores also correlate with notable textural and chemical variations. The texture of crystals (Figs. 6 and S1) is the first characteristic worth noting (Fig. 9). Most *High-T* clinopyroxene cores have euhedral habits with normal zonation pattern (80%). In contrast, the *Low-T* clinopyroxene cores mainly exhibit patchy-resorbed texture (44%) and oscillatory zoning (36%) with minor normal zoning (20%). The *Low-P* clinopyroxene cores consist of roughly the same quantity of normal zoned (50%) and patchy-resorbed (47%) textures with < 3% oscillatory zoning.

The overall compositional variation of clinopyroxenes indicates a progressive evolution of magma en route to the surface: the shallower the depth of crystallization, the lower the diopside component (Fig. 10a). However, the clinopyroxene cores of the *Low-T* group have, on average, a higher diopside component (Fig. 10a) than those of the *High-T* group, which seems at odds with their relatively low temperature estimates (ca. 1075 °C vs. 1170 °C; Fig. 8). This apparent contradiction could be explained if the *Low-T* clinopyroxene cores crystallized from magmas at higher  $P_{\text{H}_2\text{O}}$  than those

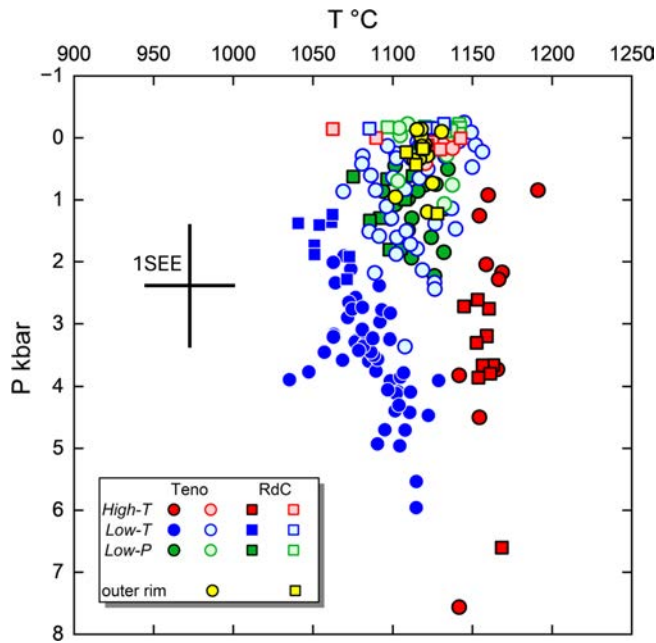


**Figure 8.**  $P$ – $T$  diagram like Fig. 7 but using only the results of the GAIA geothermobarometer and subdividing the clinopyroxene cores (and rims) according to the three different groups: *Low-T*, *High-T*, and *Low-P*. The rims have been further subdivided into rims and outer rims (see text for explanation). The 1 SEE error bars are 1 kbar and 30 °C (Chicchi et al., 2023).

of the *High-T* group because the higher the  $H_2O$  content of magma, the lower the liquidus temperature of clinopyroxene and the higher the diopside component (e.g. O’Leary et al., 2010). The occurrence of a variable amount of dissolved  $H_2O$  in mafic alkaline magmas at Tenerife is supported, for example, by Longpré et al. (2009) ( $H_2O = 0.75$  wt %–3 wt %) and could be due to differences in mantle source hydration and magmatic differentiation. Another notable chemical characteristic of the studied clinopyroxene is the generally higher kushiroite component (i.e. Ca-Tschermak:  $CaAl_2SiO_6$ ) in the *High-T* and *Low-P* clinopyroxene cores with respect to the *Low-T* group (Fig. 10b and c), which is consistent with the combined effect of pressure and temperature. High temperature and low pressure allow the expansion of the tetrahedral site of clinopyroxene favouring the  $^{IV}Al \rightarrow ^{IV}Si$  substitution (Dal Negro et al., 1982). This is not observed in the clinopyroxene rim compositions, which show a decrease in the kushiroite component from values similar to the *Low-P* clinopyroxene cores to significantly lower ones, especially in the outer rims (Fig. 10b and c). In this case, however, the reason is to be found in the decrease in  $^{VI}Al$  in the clinopyroxene structure during magma evolution (Fig. 10d). In addition to the kushiroite component, other chemical characteristics are consistent with the three outlined  $P$ – $T$  trends (Fig. 8) and extend to the rim compositions as well. The CaTi-Tschermak component generally increases with evolution (i.e. decreas-

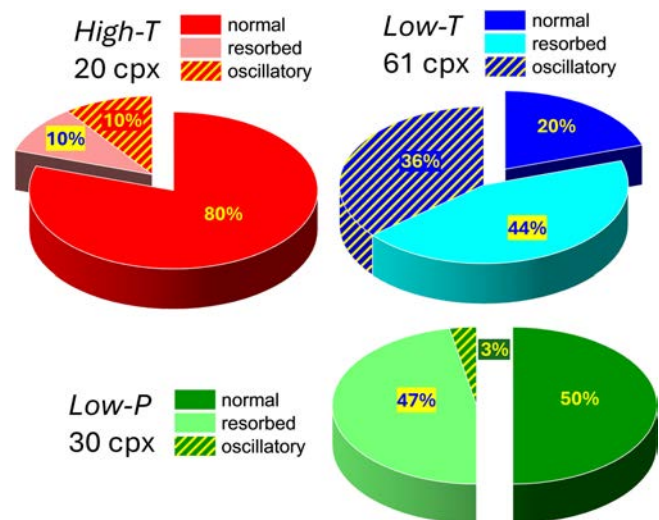


**Figure 9.** 3D pie charts reporting the distribution frequency of normal zoned, oscillatory zoned, and patchy-resorbed crystals occurring in the three groups of clinopyroxenes outlined in Fig. 8 (*Low-T*, *High-T*, and *Low-P*). The total number of clinopyroxenes (cpx) analysed for each group is also reported.

ing  $Mg\# = [100 \cdot Mg / (Mg + Fe + Mn) \text{ mol } \%]$ , Fig. 10e) and is coupled with the decrease in  $Al_{tot}/Ti$  (a.p.f.u.) (Fig. 10f). Yet, within this general evolution (clinopyroxene cores and rims), two distinct trends can be highlighted in the diagrams of the last two panels (Fig. 10e, f), distinguishing the clinopyroxenes of the *Low-T* group from those of the *High-T* and *Low-P* groups. Considering rim compositions, the clinopyroxenes of the *Low-T* group have  $Mg\# > 77\%$ , whereas those of the *High-T* and *Low-P* groups have  $Mg\# < 77\%$  (Fig. 10e, f). We are unable to clearly explain this systematic difference, but we argue that it could also be related to variable initial  $P_{H_2O}$  of the ankaramite magmas from which the cores crystallized.

Overall, it is possible to reconstruct the complex plumbing system of the Teno and Roque del Conde shield volcanoes by combining the  $P$ – $T$  estimates (Fig. 8) with the textural (Figs. 6 and 9) and chemical (Fig. 10) characteristics of the different clinopyroxene groups. The comparatively large size of *Low-T* clinopyroxene, coupled with the preponderance of patchy-resorbed cores and oscillatory zoning, suggests a relatively long residence time in deep magmatic reservoirs at low degrees of undercooling. Here, crystals grew in a context of periodic infilling of fresh magma, determining both disequilibrium conditions and oscillatory crystal growth. The pressure range of the *Low-T* clinopyroxene cores from 6 to 1 kbar implies a well-developed system of multi-level magma storage at depth, with formation of mush-rich domains (e.g. Thirlwall et al., 2000; Horn et al., 2022). The  $Mg\#$  of these clinopyroxene cores also indicates crystallization at relatively high  $P_{H_2O}$ . The occurrence of a different water content in ocean island basalt (OIB)

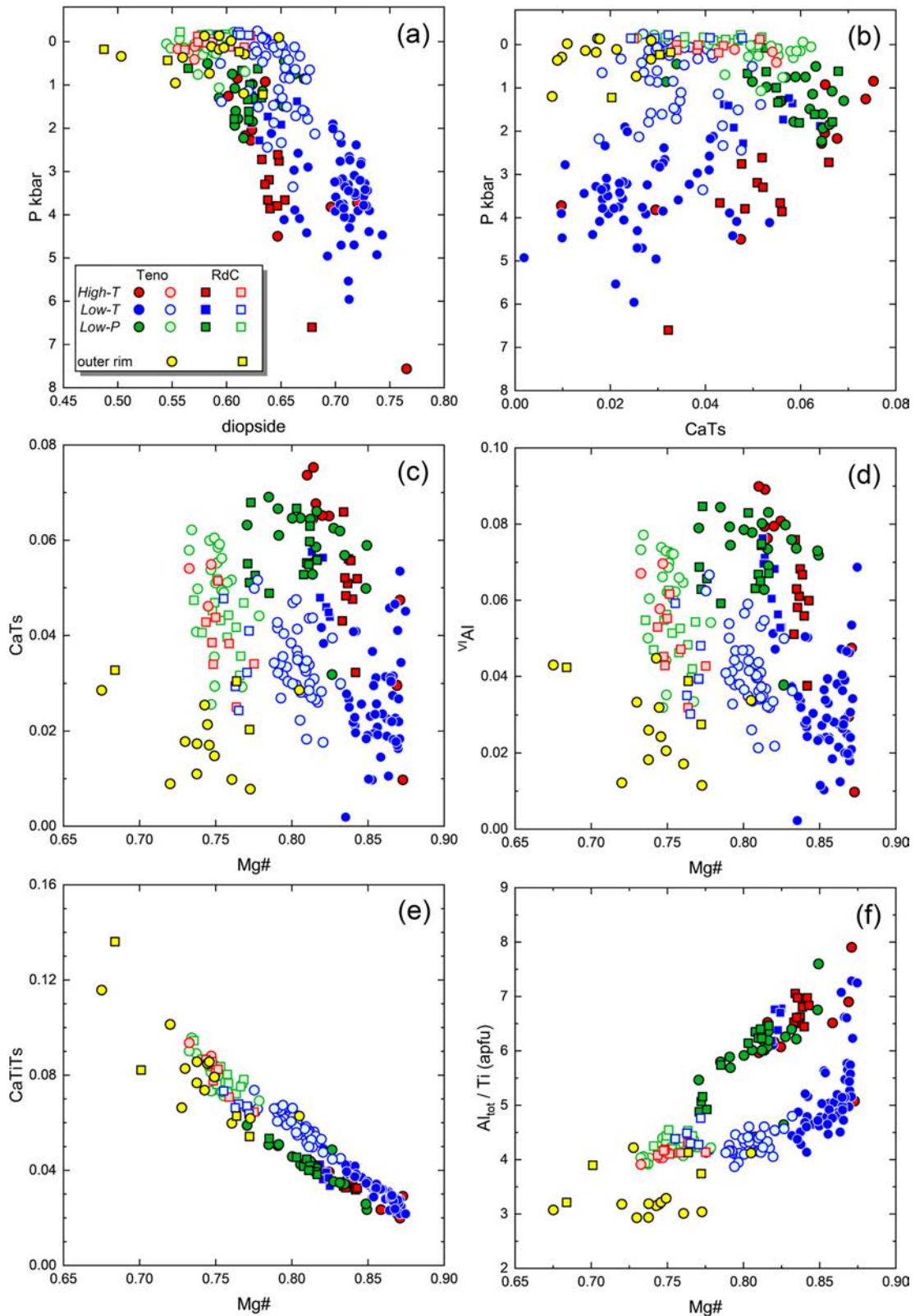


**Figure 10.** Chemical characteristics of the three groups of clinopyroxenes (see text for explanation): (a) diopside component vs.  $P$  [kbar]; (b) kushiroite component (CaTs) vs.  $P$  [kbar]; (c) Mg# vs. kushiroite; (d) Mg# vs.  $^{VI}Al$  a.p.f.u.; (e) Mg# vs. CaTi-Ts component; (f) Mg# vs.  $Al_{tot}/Ti$  (a.p.f.u.).

is not a paradox and reflects differences in mantle source hydration and magmatic differentiation. *Wet* OIB (Geiger et al., 2025) is stored in underplating zones and is ubiquitous in volcanoes of the Canary Islands and other ocean island suites (e.g. Wallace and Anderson, 1998; Gurenko and Schmincke, 2000; Dixon and Clague, 2001; Longpré et al., 2009; Deegan et al., 2012; Weis et al., 2015). The relatively small size (1–2 mm) of *High-T* clinopyroxene, along with the preponderance of normal zoned crystals and the near absence of patchy-resorbed textures, indicates rapid crystallization of these clinopyroxenes from the hot (1175 °C) feeding ankaramite magma during the rise from 8 kbar to the shallow magmatic reservoirs at 0–2 kbar. The lower Mg# than *Low-T* clinopyroxene cores suggests crystallization at relatively low  $P_{H_2O}$ . The higher kushiroite component of the *High-T* clinopyroxene cores with respect to the *Low-T* is consistent with the expansion of the tetrahedral site at higher temperatures, even at comparable pressure. This ankaramite magma, channelized en route to the surface, incorporated mush-rich domains at 6–1 kbar, causing further disequilibrium conditions (i.e. *Low-T* clinopyroxene cores). The *Low-P* clinopyroxene cores crystallized in the shallow magmatic reservoirs, as indicated by clinopyroxene rims. In this case, the high kushiroite component of the *Low-P* cores is consistent with the relatively low crystallization pressure, which also allows for a larger tetrahedral site (Dal Negro et al., 1982). These *Low-P* cores consist, in almost equal amount, of normal zoned clinopyroxenes and patchy-resorbed core clinopyroxenes (Fig. 9). The former indicates progressive crystallization, culminating in the formation of clinopyroxene rims during magma evolution; the latter is suggestive of a relatively long residence time at low degrees of undercooling in the shallow magmatic reservoirs, and the textural disequilibrium is indicative of periodic infilling of fresh magma. The occurrence of the *Low-P* clinopyroxene cores in the studied samples suggests that the *High-T* ankaramite magma en route to the surface remobilized mush-rich domains from these shallow reservoirs as well. It is worth noting that the studies on the present-day Teide–Pico Viejo plumbing system of Tenerife do not provide evidence for mafic reservoirs at shallow depth. Rather, the anatomy of the plumbing system is thought to consist of evolved phonolitic magmatic reservoirs with only short-term mafic magma injection and interaction (e.g. Andújar and Scaillet, 2012; Andújar et al., 2013; Dorado et al., 2021, 2023). However, the *Low-P* clinopyroxene cores with their patchy-resorbed texture (Figs. 6b, 9) appear to suggest the occurrence of shallow mafic reservoirs as well, at least during the volcano shield stage at 12–5 Ma.

#### 4.2 A complex plumbing system revealed by clinopyroxenes

The new geothermobarometric constraints of our study, together with the different  $P$ – $T$  trends exhibited by the analysed clinopyroxene cores (*High-T*, *Low-T*, *Low-P*; Fig. 8)

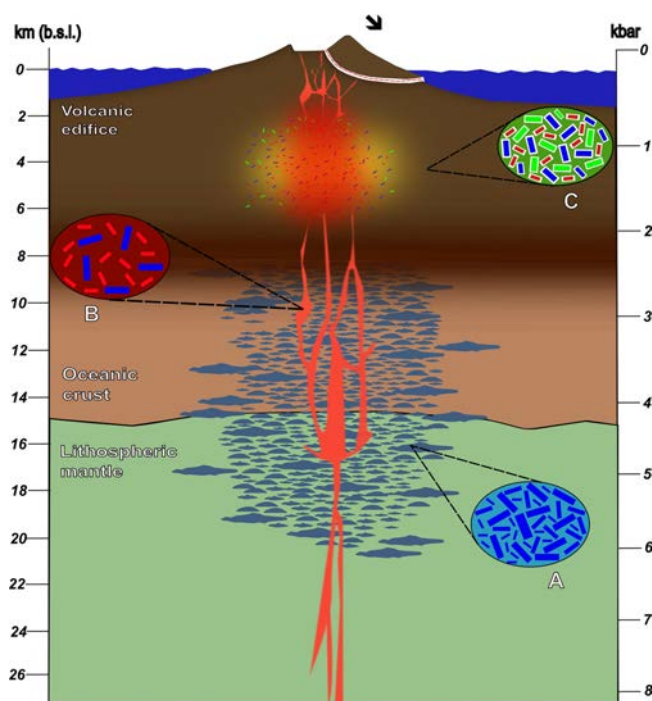


**Figure 11.** Schematic picture summarizing the ankaramite multi-level plumbing system ( $x$  axis not to scale). The colours of the crystals correspond to the different  $P$ – $T$  groups identified in Fig. 8. The three insets represent distinct stages of our model: (a) a crystal mush region (blue colour) hosting *Low-T* clinopyroxenes; (b) rising of hot magma with crystallization of the *High-T* clinopyroxenes en route to the surface (red colour) and entrapment of *Low-T* clinopyroxenes from crystal mushes; (c) crystallization of *Low-P* group clinopyroxenes in shallow magma chambers where clinopyroxenes of the three different groups are stored before the eruption. The rims (represented in white) of the entire suite of clinopyroxenes crystallize in these shallow reservoirs. The eruption is eventually induced by massive sector collapse, which causes the depressurization of the plumbing system.

and their textural and compositional variations (Figs. 6, 9, 10), allow us to develop a stratigraphic model for the anatomy of the plumbing system of ankaramites at Tenerife (Fig. 11).

We converted the pressure estimates (kbar) into depth (km) using the log of the stratigraphic sequence and the average density of each lithotype from the literature (Banda et al., 1981; Watts et al., 1997; Ablay and Kearey, 2000; Collier and Watts, 2001). The lithospheric mantle has a density of  $3.2 \text{ t m}^{-3}$ , and the Moho is set at ca. 15 km b.s.l.; the oceanic crust has a thickness of ca. 6.5–7 km with a density of  $2.9 \text{ t m}^{-3}$ ; the base of the volcano is located at 8 km b.s.l., as suggested by Watts et al. (1997) and Dañobeitia and Canales (2000). The altitude of the Teno volcanic edifice was set at the present-day altitude of 1.3 km a.s.l., with an average density of  $2.6 \text{ t m}^{-3}$  (Watts et al., 1997; Collier and Watts, 2001). Contextualizing our results with available

geophysical data on Tenerife, the parental magma found a physical density barrier at the depth corresponding to the Moho geophysical discontinuity (ca. 4.2 kbar or 15 km b.s.l.), which promoted magma stagnation between the lithospheric mantle (ca.  $3.2 \text{ t m}^{-3}$ ) and the oceanic crust (ca.  $2.9 \text{ t m}^{-3}$ ). The formation of crystal mushes, represented by the *Low-T* and partly *Low-P* clinopyroxene cores, likely took place during the shield stage evolution, with magma stagnation at different crustal levels. These multi-level magma storage reservoirs are present throughout the oceanic crust and the upper portion of the lithospheric mantle (Fig. 11), producing large volumes of mafic cumulates in response to a long residence time in relatively cold and hydrous magmatic reservoirs (1025–1125 °C) (e.g. Thirlwall et al., 2000; Horn et al., 2022). During the cycle of this activity, batches of mafic, less hydrated magma (1150–1200 °C) ascending from the mantle not only continuously crystallized the *High-T* clinopyroxenes but also tore off crystal mush portions (*Low-T* clinopyroxenes) and carried them up into the shallower magmatic reservoirs where *Low-P* clinopyroxenes crystallized (Fig. 11). Eventually, the erupting magma brought to the surface all the suites of crystals belonging to the different groups which were situated in the multi-level magmatic reservoirs (Fig. 11), resulting in a complex and heterogeneous clinopyroxene cargo recognized in the studied ankaramites.

#### 4.3 Comparison with previous estimates and with other volcano shield stage ankaramites

The complex plumbing system developed during the shield stage at Tenerife and proposed in this study is somehow in contradiction with the detailed work of Longpré et al. (2008, 2009). These authors proposed that magma storage of ankaramites is confined to a depth range between 20 and 45 km b.s.l., whereas in our model the depths of magma storage are much shallower (< 20 km b.s.l., Fig. 11). To solve this dichotomy, we explored the results related to the plumbing systems of other islands of the Canary Islands in their volcano shield stage: La Palma and El Hierro ankaramites and basanites (Weis et al., 2015; Geiger et al., 2025). In addition to the main upper-mantle reservoirs (18–32 km b.s.l.), ankaramites and basanite on these two western islands of the Canary Islands encountered two shallower storage levels, the so-called *magma underplating zone* (10–15 km b.s.l.) and the *intrusive core complex* (5–10 km b.s.l.) (Weis et al., 2015). The ankaramites studied by Geiger et al. (2025) at El Hierro recorded crystallization pressure between 1.6 and 7.6 kbar (5–26 km b.s.l.) with a cluster around 20–23 km, consistent with a major underplating zone at the crust–mantle boundary and minor storage zones at shallow depths. El Hierro ankaramites were also modelled using a thermodynamic approach by Prieto-Torrell et al. (2025). Their results demonstrated that ankaramites represent crystal mushes compatible with a crystal fractionation and accumulation model at

4 kbar (ca. 14 km b.s.l.) and 1 wt % H<sub>2</sub>O. Clinopyroxene–melt equilibria of basanites at La Palma (Klügel et al., 2005) recorded pressures of 4.1–7.7 kbar, reflecting a major fractionation level at 15–26 km b.s.l., whereas fluid inclusions in phenocrysts and xenoliths yielded pressures of 2.4–4.7 kbar, interpreted as an underplating zone at 7–14 km b.s.l. The study of Galipp et al. (2006), always at La Palma, revealed two distinct storage and underplating levels within the upper mantle (clinopyroxene–melt geobarometry) and within the lower crust (fluid inclusion geobarometry in olivine and clinopyroxene phenocrysts). Interestingly, both the mantle and the crustal storage zones migrated to shallower levels from 1.0 Ma to the present, namely, from ca. 6–10 to 5–7.8 kbar and from 4–5 to 2.6–3.2 kbar, respectively. At Tenerife, a magnetotelluric survey (Piña-Varas et al., 2018) provided evidence for the occurrence of a large-scale deep mafic reservoir at > 8 km b.s.l. Horn et al. (2022) reported the results of mafic–ultramafic nodules occurring in the 312 ka Fasnía eruption. These nodules represent a crystal framework in a magma mush reservoir located at 6–7 km b.s.l. (ca. 2 kbar) and 13–14 km b.s.l. (ca. 3.5–4 kbar) in agreement with gravimetric studies (Ablay and Kearey, 2000; Araña et al., 2000) and geobarometry (Neumann et al., 1999). These mafic–ultramafic nodules were interpreted as cumulates corresponding to regions where mafic magma tended to stagnate during the Miocene shield stage evolution, consistent with the results obtained in our study (Fig. 11). Interestingly, another example of ankaramite eruption during the volcano shield stage is related to the Maui volcano complex formed by the hotspot track of Hawaii (Hammer et al., 2016). The authors reported that the ankaramite magma storage zones are confined to the volcanic shield and oceanic crust levels up to 15 km b.s.l. Thus, as illustrated in the abovementioned studies, the results presented in this work on ankaramite magma storage zones during the volcano shield stage at Tenerife (Fig. 11) are compatible with other plumbing systems of the Canary Islands and Hawaii, although the deep storage zones reported by Longpré et al. (2008) cannot be ruled out and may complement the magma storage zones at shallower levels determined with GAIA (Fig. 11). However, dense crystal mushes such as ankaramites (ca.  $3 \text{ t m}^{-3}$ ) stored at mantle depths (> 20 km) are unlikely to ascend and erupt, since the load of the volcanic edifice and oceanic crust represents a physical density barrier (e.g. Pinel and Jaupart, 2000; Cassidy et al., 2015). The eruption of ankaramite requires a significant decompression effect caused, for example, by giant landslides or flank collapses, which remove parts of the load, shift the density limit, and permit dense magmas to ascend and erupt (e.g. Manconi et al., 2009; Cassidy et al., 2015). Thus, we can tentatively speculate that the probability of erupting ankaramites located in shallow magmatic reservoirs as predicted by our geothermobarometer (Fig. 11) is much more likely than eruption of ankaramites stored at mantle depths (> 20 km).

## 5 Conclusions

Our study employed a novel clinopyroxene-only machine learning geothermobarometer and a geobarometer based upon structural parameters of clinopyroxene to unravel the magma plumbing system of ankaramites that erupted during the volcano shield stage at Tenerife. Clinopyroxenes have three different zonation textures, characterized by small crystals (< 1–2 mm) with normal zonation and large crystals (> 1 cm) with both resorbed-patchy cores and oscillatory zoning. The chemical and textural diversity of clinopyroxene, particularly the variation in diopside, Mg#, and Al/Ti (a.p.f.u.), highlights the influence of variable H<sub>2</sub>O content and magmatic differentiation processes in ankaramites. Clinopyroxene rims yield a major crystallization frequency at 0–2 kbar, whereas clinopyroxene cores show a continuous crystallization between 1 and 8 kbar. In particular, clinopyroxene cores record a complex magmatic history, revealing three distinct *P–T* groups corresponding to different storage and crystallization environments. The *Low-T* group represents a set of clinopyroxene cores crystallized from relatively high *P*<sub>H<sub>2</sub>O</sub> magmas. Their resorbed-patchy textures testify to the chemical disequilibria between crystals and host magma and suggest the occurrence of an extended crystal mush at 2–6 kbar. The small-sized (< 1–2 mm), euhedral crystal habits and normal zonation of the *High-T* group clinopyroxene cores suggest a direct crystallization from the carrier hot magma during rapid adiabatic rising from ca. 8 up to 1 kbar. The *Low-P* group clinopyroxene cores are clustered into the same domain of the rims (0–2 kbar), suggesting a shallow level of magma storage. In summary, the model we propose for the plumbing system of ankaramite magma at Tenerife consists of a hot carrier parental mafic magma (*High-T* group clinopyroxenes), which, during its rise from depth (> 20 km b.s.l.), incorporates portions of crystal mush domains (*Low-T* group clinopyroxenes) and conveys these two suites of crystals up to the shallower magmatic reservoirs (0–7 km). At these depths, new clinopyroxene cores (*Low-P* group) crystallize together and in the same *P–T* conditions as those of the rims from the other groups, which are often (especially the *Low-T* group) in conditions of chemical disequilibrium, as testified by their resorbed and patchy textures. Notably, the results indicate that the volcano shield stage of Tenerife is characterized by multi-level storage, with magma batches stalling at the density barrier near the Moho and interacting with crystal mushes en route to the surface. These findings not only align with but also extend previous geothermobarometric studies and refine our understanding of the ankaramite plumbing system at Tenerife. The consistency with geobarometric estimates in other volcano shield stages of the Canary Islands and Hawaii is remarkable and offers new insights into magma storage complexities.

Finally, our approach and findings encourage the broader application of machine learning models in petrology, fos-

tering interdisciplinary collaborations that combine mineral chemistry, geophysics, and computational techniques.

**Data availability.** The authors confirm that the data supporting the findings of this study are available within the article (Sect. 4, Figs. 5–10) and its Supplement. Crystallographic information files can be made available upon request.

**Supplement.** The supplement related to this article is available online at <https://doi.org/10.5194/ejm-37-747-2025-supplement>.

**Author contributions.** Conceptualization: LuB, ST; investigation: LoB, MM, TC; methodology: LoB, LuB, ST, MM, TC; supervision: LuB, ST; validation: RA, LuB, ST; writing – original draft: LoB; writing – review & editing: RA, LoB, LuB, MM, ST. All authors read and approved the final article.

**Competing interests.** At least one of the (co-)authors is a member of the editorial board of the *European Journal of Mineralogy*. The peer-review process was guided by an independent editor, and the authors also have no other competing interests to declare.

**Disclaimer.** Publisher's note: Copernicus Publications remains neutral with regard to jurisdictional claims made in the text, published maps, institutional affiliations, or any other geographical representation in this paper. While Copernicus Publications makes every effort to include appropriate place names, the final responsibility lies with the authors. Views expressed in the text are those of the authors and do not necessarily reflect the views of the publisher.

**Special issue statement.** This article is part of the special issue “Celebrating the outstanding contribution of Paola Bonazzi to mineralogy”. It is not associated with a conference.

**Acknowledgements.** The authors thank Martina Casalini and Raffaello Cioni for their support during the fieldwork related to this research. The clarity of the original manuscript was greatly improved by the suggestions, comments, and criticism of Olaya Dorado and the anonymous reviewer and by the editorial handling of Marco Pasero and Elisabetta Rampone. The authors acknowledge CRIST, Centro di Studi per la Cristallografia Strutturale, Università degli Studi di Firenze (Italy), for X-ray diffraction measurements. Scanning electron microscope data were collected at MEMA Centro di Servizi di Microscopia Elettronica e Microanalisi, Università degli Studi di Firenze (Italy). Electron microprobe analyses were carried out at LaMA, Laboratorio di MicroAnalisi, Università degli Studi di Firenze (Italy). This work is dedicated to the memory of our esteemed colleague and dear friend Paola Bonazzi, whose brilliance, integrity, and unwavering curiosity left an indelible mark on our research and our lives. Her contributions to mineralogy were both profound and inspiring, and her absence is deeply felt. Though

she left us far too soon, her spirit continues to guide our work and reminds us of the passion and purpose that science can embody.

**Financial support.** This work has been funded by research grants from the University of Firenze (Fondo Ateneo ex-60%) to Simone Tommasini. Lorenzo Barni, Luca Bindi, and Marta Morana acknowledge financial support by HERMES project no. 2022R35X8Z, and Riccardo Avanzinelli acknowledges financial support by TRANSIENT project no. 2022PC9NME (MUR-PRIN 2022).

**Review statement.** This paper was edited by Marco Pasero and reviewed by Olaya Dorado and one anonymous referee.

## References

- Ablay, G. J. and Kearey, P.: Gravity constraints on the structure and volcanic evolution of Tenerife, Canary Islands, *J. Geophys. Res.-Sol. Ea.*, 105, 5783–5796, <https://doi.org/10.1029/1999JB900404>, 2000.
- Ancochea, E., Fúster, J., Ibarrola, E., Cendrero, A., Coello, J., Hernan, F., Cantagrel, J. M., and Jamond, C.: Volcanic evolution of the island of Tenerife (Canary Islands) in the light of new K-Ar data, *J. Volcanol. Geoth. Res.*, 44, 231–249, [https://doi.org/10.1016/0377-0273\(90\)90019-C](https://doi.org/10.1016/0377-0273(90)90019-C), 1990.
- Andújar, J. and Scaillet, B.: Experimental Constraints on Parameters Controlling the Difference in the Eruptive Dynamics of Phonolitic Magmas: the Case of Tenerife (Canary Islands), *J. Petrol.*, 53, 1777–1806, <https://doi.org/10.1093/petrology/egs033>, 2012.
- Andújar, J., Costa, F., and Scaillet, B.: Storage conditions and eruptive dynamics of central versus flank eruptions in volcanic islands: The case of Tenerife (Canary Islands, Spain), *J. Volcanol. Geoth. Res.*, 260, 62–79, <https://doi.org/10.1016/j.jvolgeores.2013.05.004>, 2013.
- Araña, V., Camacho, A. G., Garcia, A., Montesinos, F. G., Blanco, I., Vieira, R., and Felpeto, A.: Internal structure of Tenerife (Canary Islands) based on gravity, aeromagnetic and volcanological data, *J. Volcanol. Geoth. Res.*, 103, 43–64, [https://doi.org/10.1016/S0377-0273\(00\)00215-8](https://doi.org/10.1016/S0377-0273(00)00215-8), 2000.
- Banda, E., Dañobeitia, J. J., Suriñach, E., and Ansoorge, J.: Features of crustal structure under the Canary Islands, *Earth Planet. Sc. Lett.*, 55, 11–24, [https://doi.org/10.1016/0012-821X\(81\)90082-0](https://doi.org/10.1016/0012-821X(81)90082-0), 1981.
- Brey, G. P. and Kohler, T.: Geothermobarometry in Four-phase Lherzolites II. New Thermobarometers, and Practical Assessment of Existing Thermobarometers, *J. Petrol.*, 31, 1353–1378, <https://doi.org/10.1093/petrology/31.6.1353>, 1990.
- Cashman, K. V., Sparks, R. S. J., and Blundy, J. D.: Vertically extensive and unstable magmatic systems: a unified view of igneous processes, *Science*, 355, eaag3055, <https://doi.org/10.1126/science.aag3055>, 2017.
- Cassidy, M., Watt, S. F. L., Talling, P. J., Palmer, M. R., Edmonds, M., Jutzeler, M., Wall-Palmer, D., Manga, M., Coussens, M., Gernon, T., Taylor, R. N., Michalik, A., Inglis, E., Breitkreuz, C., Le Friant, A., Ishizuka, O., Boudon, G., McCanta, M. C., Adachi, T., Hornbach, M. J., Colas, S. L., Endo, D., Fujinawa, A., Kataoka, K. S., Maeno, F., Tamura, Y., and Wang, F.: Rapid onset of mafic magmatism facilitated by volcanic edifice collapse, *Geophys. Res. Lett.*, 42, 4778–4785, 2015.
- Chatterjee, N., Bhattacharji, S., and Fein, C.: Depth of alkalic magma reservoirs below Kolekole cinder cone, Southwest rift zone, East Maui, Hawaii, *J. Volcanol. Geoth. Res.*, 145, 1–22, <https://doi.org/10.1016/j.jvolgeores.2005.01.001>, 2005.
- Chicchi, L., Bindi, L., Fanelli, D., and Tommasini, S.: Frontiers of thermobarometry: GAIA, a novel Deep Learning-based tool for volcano plumbing systems, *Earth Planet. Sc. Lett.*, 620, 118352, <https://doi.org/10.1016/j.epsl.2023.118352>, 2023.
- Collier, J. S. and Watts, A. B.: Lithospheric response to volcanic loading by the Canary Islands: constraints from seismic reflection data in their flexural moat, *Geophys. J. Int.*, 147, 660–676, <https://doi.org/10.1046/j.0956-540x.2001.01506.x>, 2001.
- Dal Negro, A., Carbonin, S., Molin, G. M., Cundari, A., and Piccirillo, E. M. Intracrystalline cation distribution in natural clinopyroxenes of tholeiitic, transitional, and alkaline basaltic rocks, in: *Advances in Physical Geochemistry*, vol. 2, Springer New York, New York, NY, 117–150, [https://doi.org/10.1007/978-1-4612-5683-0\\_3](https://doi.org/10.1007/978-1-4612-5683-0_3), 1982.
- Dañobeitia, J. J., and Canales, J. P.: Magmatic underplating in the Canary Archipelago. *J. Volcanol. Geoth. Res.*, 103, 27–41, [https://doi.org/10.1016/S0377-0273\(00\)00214-6](https://doi.org/10.1016/S0377-0273(00)00214-6), 2000.
- Deegan, F. M., Troll, V. R., Barker, A. K., Harris, C., Chadwick, J. P., Carracedo, J. C., and Delcamp, A.: Crustal versus source processes recorded in dykes from the Northeast volcanic rift zone of Tenerife, Canary Islands, *Chem. Geol.*, 334, 324–344, 2012.
- Delvigne, J., Bisdom, E. B. A., Sleeman, J., and Stoops, G.: Olivines, their pseudomorphs and secondary products, *Pedologie*, 29, 247–309, 1979.
- Dixon, J. E. and Clague, D. A.: Volatiles in basaltic glasses from Loihi Seamount, Hawaii: Evidence for a relatively dry plume component, *J. Petrol.*, 42, 627–654, 2001.
- Dorado, O., Andújar, J., Martí, J., and Geyer, A.: Pre-eruptive conditions at satellite vent eruptions at Teide-Pico Viejo complex (Tenerife, Canary Islands), *Lithos*, 396, 106193, <https://doi.org/10.1016/j.lithos.2021.106193>, 2021.
- Dorado, O., Wolff, J. A., Ramos, F. C., and Martí, J.: Ba, Sr, and Rb feldspar/melt partitioning in recent eruptions from Teide-Pico Viejo volcanic complex, Tenerife: New insights into pre-eruptive processes, *Front. Earth Sci.*, 11, 1155724, <https://doi.org/10.3389/feart.2023.1155724>, 2023.
- Fúster, J. M., Araña, V., Brandle, J. L., Navarro, J. M., Alonso, U., and Aparicio, A.: Geology and Volcanology of the Canary Islands: Tenerife, Inst. Lucas Mallada, CSIC, Madrid, 218 pp., 1968.
- Galipp, K., Klügel, A., and Hansteen, T. H.: Changing depths of magma fractionation and stagnation during the evolution of an oceanic island volcano: La Palma (Canary Islands), *J. Volcanol. Geoth. Res.*, 155, 285–306, <https://doi.org/10.1016/j.jvolgeores.2006.04.002>, 2006.
- Geiger, H., Weis, F., Troll, V. R., Deegan, F. M., Skogby, H., and Carracedo, J. C.: Explosive ocean island volcanism explained by high magmatic water content determined through nominally anhydrous minerals, *Geochem. Geophys. Geos.*, 26, e2024GC012013, <https://doi.org/10.1029/2024GC012013>, 2025.

- Guillou, H., Carracedo, J. C., Pérez Torrado, F., and Rodríguez Badiola, E.: K-Ar ages and magnetic stratigraphy of a hotspot-induced, fast grown oceanic island: El Hierro, Canary Islands, *J. Volcanol. Geoth. Res.*, 73, 141–155, [https://doi.org/10.1016/0377-0273\(96\)00021-2](https://doi.org/10.1016/0377-0273(96)00021-2), 1996.
- Guillou, H., Carracedo, J. C., Paris, R., and Pérez Torrado, F. J.: Implications for the early shield-stage evolution of Tenerife from K/Ar ages and magnetic stratigraphy, *Earth Planet. Sc. Lett.*, 222, 599–614, <https://doi.org/10.1016/j.epsl.2004.03.012>, 2004.
- Gurenko, A. A. and Schmincke, H.: S concentrations and its speciation in Miocene basaltic magmas north and south of Gran Canaria (Canary Islands): constraints from glass inclusions in olivine and clinopyroxene, *Geochim. Cosmochim. Ac.*, 64, 2321–2337, 2000.
- Hammer, J., Jacob, S., Welsch, B., Hellebrand, E., and Sinton, J.: Clinopyroxene in postshield Haleakala ankaramite: 1. Efficacy of thermobarometry, *Contrib. Mineral. Petrol.*, 171, 7, <https://doi.org/10.1007/s00410-015-1212-x>, 2016.
- Hirschmann, M. M., Ghiorso, M. S., Davis, F. A., Gordon, S. M., Mukherjee, S., Grove, T. L., Krawczynski, M., Medard, E., and Till, C. B.: Library of Experimental Phase Relations (LEPR): A database and Web portal for experimental magmatic phase equilibria data, *Geochem. Geophys. Geosy.*, 9, 2007GC001894, <https://doi.org/10.1029/2007GC001894>, 2008.
- Horn, E. L., Taylor, R. N., Gernon, T. M., Stock, M. J., and Farley, E. R.: Composition and petrology of a mush-bearing magma reservoir beneath Tenerife. *J. Petrol.*, 63, egac095, <https://doi.org/10.1093/ptrology/egac095>, 2022.
- Klügel, A., Hansteen, T. H., and Galipp, K.: Magma storage and underplating beneath Cumbre Vieja volcano, La Palma (Canary Islands), *Earth Planet. Sc. Lett.*, 236, 211–226, <https://doi.org/10.1016/j.epsl.2005.04.006>, 2005.
- Lacroix, A.: La constitution des roches volcaniques de l'Extrême Nord de Madagascar et de Nosy Bé; les ankaramites de Madagascar en général, *Comptes Rendus Académie des Sciences, Paris*, 163, 253–258, 1916.
- Longpré, M.-A., Troll, V. R., and Hansteen, T. H.: Upper mantle magma storage and transport under a Canarian shield-volcano, Teno, Tenerife (Spain): Teno magma plumbing, *J. Geophys. Res.-Sol. Ea.*, 113, <https://doi.org/10.1029/2007JB005422>, 2008.
- Longpré, M.-A., Troll, V. R., Walter, T. R., and Hansteen, T. H.: Volcanic and geochemical evolution of the Teno massif, Tenerife, Canary Islands: Some repercussions of giant landslides on ocean island magmatism: Teno volcanism and effects on landslides, *Geochem. Geophys. Geosy.*, 10, <https://doi.org/10.1029/2009GC002892>, 2009.
- Manconi, A., Longpré, M.-A., Walter, T. R., Troll, V. R., and Hansteen, T. H.: The effects of flank collapses on volcano plumbing systems, *Geology*, 37, 1099–1102, <https://doi.org/10.1130/G30104A.1>, 2009.
- McDougall, I. and Schmincke, H.-U.: Geochronology of Gran Canaria, Canary Islands: Age of shield building volcanism and other magmatic phases, *B. Volcanol.*, 40, 57–77, <https://doi.org/10.1007/BF02599829>, 1976.
- Müller, R. D., Roest, W. R., Royer, J.-Y., Gahagan, L. M., and Sclater, J. G.: Digital isochrons of the world's ocean floor, *J. Geophys. Res.*, 102, 3211–3214, <https://doi.org/10.1029/96JB01781>, 1997.
- Neumann, E.-R., Wulff-Pedersen, E., Simonsen, S. L., Pearson, N. J., Marti, J., and Mitjavila, J.: Evidence for Fractional Crystallization of Periodically Refilled Magma Chambers in Tenerife, Canary Islands, *J. Petrol.*, 40, 1089–1123, <https://doi.org/10.1093/ptroj/40.7.1089>, 1999.
- Nimis, P.: A clinopyroxene geobarometer for basaltic systems based on crystal-structure modeling, *Contrib. Mineral. Petrol.*, 121, 115–125, <https://doi.org/10.1007/s004100050093>, 1995.
- Nimis, P. and Ulmer, P.: Clinopyroxene geobarometry of magmatic rocks Part 1: An expanded structural geobarometer for anhydrous and hydrous, basic and ultrabasic systems, *Contrib. Mineral. Petrol.*, 133, 122–135, <https://doi.org/10.1007/s004100050442>, 1998.
- O'Leary, J. A., Gaetani, G. A., and Hauri, E. H.: The effect of tetrahedral Al<sup>3+</sup> on the partitioning of water between clinopyroxene and silicate melt, *Earth Planet. Sc. Lett.*, 297, 111–120, <https://doi.org/10.1016/j.epsl.2010.06.011>, 2010.
- Petrelli, M.: *Machine Learning for Earth Sciences*, Springer Nature Switzerland AG 2023, Hardcover, ISBN 978-3-031-517 35113-6, 2023.
- Piña-Varas, P., Ledo, J., Queralt, P., Marcuello, A., and Perez, N.: On the detectability of Teide volcano magma chambers (Tenerife, Canary Islands) with magnetotelluric data, *Earth Planet. Space*, 70, 14, <https://doi.org/10.1186/s40623-018-0783-y>, 2018.
- Pinel, V. and Jaupart, C.: The effect of edifice load on magma ascent beneath a volcano, *Philos. T. Roy. Soc. A*, 358, 1515–1532, 2000.
- Prieto-Torrell, C., Albert, H., Aulinas, M., González-Esvertit, E., Arienzo, I., Gisbert, G., Troll, V. R., Fernandez-Turile, J.-L., Rodríguez-Gonzalez, A., and Perez-Torrado, F. J.: Mush system heterogeneities control magma composition and eruptive style on the Ocean Island of El Hierro, Canary Islands, *Contrib. Mineral. Petr.*, 180, <https://doi.org/10.1007/s00410-025-02216-6>, 2025.
- Putirka, K. D.: Thermometers and barometers for volcanic systems, *Rev. Mineral. Geochem.*, 69, 61–120, 2008.
- Sainz-Maza Aparicio, S., Martí, J., Montesinos, F. G., Borreguero Gómez, A., Pereda De Pablo, J., Vaquero Fernández, P., and Calvo García-Maroto, M.: Gravimetric study of the shallow basaltic plumbing system of Tenerife, Canary Islands, *Phys. Earth Planet. Int.*, 297, 106319, <https://doi.org/10.1016/j.pepi.2019.106319>, 2019.
- Schmidt, M. W., Green, D. H., and Hibberson, W. O.: Ultra-calcic magmas generated from Ca-depleted mantle: an experimental study on the origin of ankaramites, *J. Petrol.*, 45, 531–554, 2004.
- Thirlwall, M. F., Singer, B. S., and Marriner, G. F.: 39 Ar–40 Ar ages and geochemistry of the basaltic shield stage of Tenerife, Canary Islands, Spain, *J. Volcanol. Geoth. Res.*, 103, 247–297, [https://doi.org/10.1016/S0377-0273\(00\)00227-4](https://doi.org/10.1016/S0377-0273(00)00227-4), 2000.
- Ubide, T., Larrea, P., Becerril, L., and Galé, C.: Volcanic plumbing filters on ocean-island basalt geochemistry: *Geology*, 50, 26–31, <https://doi.org/10.1130/G49224.1>, 2021.
- Wallace, P. J. and Anderson Jr., A. T.: Effects of eruption and lava drainback on the H<sub>2</sub>O contents of basaltic magmas at Kilauea Volcano, *B. Volcanol.*, 59, 327–344, 1998.
- Walter, T. R. and Schmincke, H. U.: Rifting, recurrent landsliding and Miocene structural reorganization on NW Tenerife (Canary Islands), *Int. J. Earth Sci.*, 91, 615–628, <https://doi.org/10.1007/s00531-001-0245-8>, 2002.
- Watts, A. B., Peirce, C., Collier, J., Dalwood, R., Canales, J. P., and Henstock, T. J.: A seismic study of lithospheric flexure in

the vicinity of Tenerife, Canary Islands, *Earth Planet. Sc. Lett.*, 146, 431–447, [https://doi.org/10.1016/S0012-821X\(96\)00249-X](https://doi.org/10.1016/S0012-821X(96)00249-X), 1997.

Weis, F. A., Skogby, H., Troll, V. R., Deegan, F. M., and Dahren, B.: Magmatic water contents determined through clinopyroxene: Examples from the Western Canary Islands, Spain, *Geochem. Geophys. Geosy.*, 16, 2127–2146, 2015.